CHAPTER-1

INTRODUCTION

1.1 Motivation for Research

During the last two decades, studies on the spectroscopic properties of rare-earth (RE) ions have produced extensive information on laser and luminescent materials. Luminescent devices have now become the integral part of human daily life. Even a single moment cannot be spent without luminescent devices. Some of the luminescent devices are fluorescent lamps, light-emitting diodes (LEDs), high-definition television (HDTV) screens, and commercial display panels (DPs). Phosphors activated by Eu^{3+}, Eu^{2+}, and Tb^{3+} ions are used for lighting and displays. Er^{3+}- and Yb^{3+}-doped glasses are used for infrared-to-visible upconversion. RE-doped materials represent a lion share of the lighting market [Shionoya, et al. (1998)]. In general, white-light LED contains a RE-doped phosphor coating over the blue-emitting semiconductor diode. RE ions absorb UV–visible radiation and emit at a higher wavelength region (downconversion). This downconversion emission property is used in the optical devices mentioned above. Moreover, RE ions have high luminescence efficiencies and sharp emission bands in a wide range of optical spectrum [Dieke (1968)]. Along with the downconversion property, the RE ions can also upconvert the incident radiation, i.e., they can emit radiations of lower wavelength than the exciting radiation. This property has found prolific application in various areas, and intensive research is underway to achieve materials with high upconversion emission [Hoppe, et al. (1998)]. The upconversion materials need to be improved in terms of material stability, emission efficiency, color purity, etc.

Owing to new developments in materials science, REs have great potential in the future world of nanotechnologies for instance. RE ion-doped nanoparticles and nanomaterials are known as nanophosphors. They show some new interesting properties that were not observed in bulk materials, leading to newer applications, and thus "nanophosphors" are the future products [Bhargava, et al. (1996)].

Research in this direction is still in its infancy, and this study is motivated by current research trends on up and downconversion phosphors [Shionoya, et al. (1998) and Yang, et al. (2005)].

The chapter starts with a short survey on the luminescence spectroscopy of RE ions and their quantum mechanical results on the energy-level splitting in free form

and solids. The chapter concludes with an overview on the current research trends on up and downconversion phosphors.

1.2 Luminescence of Materials

"Luminescence" is a light-related phenomenon exhibited by a variety of materials when they absorb energy. The name originates from the Latin word *lumen* meaning light. The term "luminescenz" was first used in 1888 by a German physicist Eilhard Wiedemann for "all those phenomena of light which are not solely conditioned by the rise in temperature". He further proposed that a luminous substance becomes luminous by the action of an external agency that does not involve a rise in temperature. Now, *luminescence* is a generic term for electromagnetic radiation, usually in the form of visible light, emitted as a consequence of an atomic or molecular excitation. It is often described as "cold light" to distinguish it from incandescent light emission. Substantial observations and discoveries have been made including the luminescence from RE and transition-metal-ion-doped inorganic materials in the last two centuries; these materials were named as "phosphors" that absorb and store energy and finally convert the energy to light [Yen, et al. (2006)]. Luminescent materials can be excited by different methods of energy absorption, and are therefore classified according to their mode of excitation. The various types of luminescence were categorized in the 19th century as chemiluminescence, thermoluminescence, electroluminescence, photoluminescence, radioluminescence, and X-ray luminescence [Harvey (1957)]. Another classification of luminescence is fluorescence and phosphorescence, considering the time of deactivation of the system after the exciting radiation is switched off. In fluorescence, the emission of light occurs immediately after the illumination, whereas in phosphorescence, the emission persists even after the source of illumination is removed.

A phosphor is usually comprised of a host crystal material and one or more intentionally introduced impurities, called activators. The concentration of activators can be as low as tens of ppm for a donor–acceptor system, or can be as high as 20% in weight for single RE dopants. The band gap of a phosphor material is generally selected as larger than 3 eV to make the material transparent in the visible range. Therefore, either a wide-band-gap semiconductor or an insulator material is suitable. Luminescence is the emission of electromagnetic radiation (photon) involving a radiative transition between the energy levels of a material after absorbing energy. The luminescence of phosphors can be explained by two mechanisms **[**Shionoya, et al. (1998)**,** Feldmann, et al. (2003)**]**: (i) luminescence from the localized centers and (ii) luminescence of the semiconductors.

In the case of luminescent centers, the transitions occur between the energy levels of single ions such as Eu^{3+} in Y_2O_3: Eu^{3+} and Mn^{2+} in ZnS: Mn^{2+}. Excitation and emission can be localized on one center (called an activator) (Figure 1.1a) or they can be separated from each other: excitation of the sensitizer (S) is followed by the emission of the activator (A) (Figure 1.1b). For example, Ce^{3+} is the sensitizer, and Tb^{3+} is the activator in $LaPO_4$: Ce^{3+}, Tb^{3+}. The luminescence in semiconductors normally occurs, after band-to-band excitation, between the impurity states within the band gap. Figure 1(c) shows the luminescence emission from a semiconductor.

In this thesis, the photon-induced luminescences from RE ions in various solid host matrices have been studied. The most fascinating feature of the RE ions is their narrow emission bands covering a spectral range from ultraviolet to visible and near-infrared (NIR) regions, photoluminescence, and long-lived decay levels. RE ions have higher emission cross-sections and a wider range of emission spectrum in the UV–visible–NIR region, which are very useful for lasers, telecommunications, display devices, switching devices, and optical amplifiers.

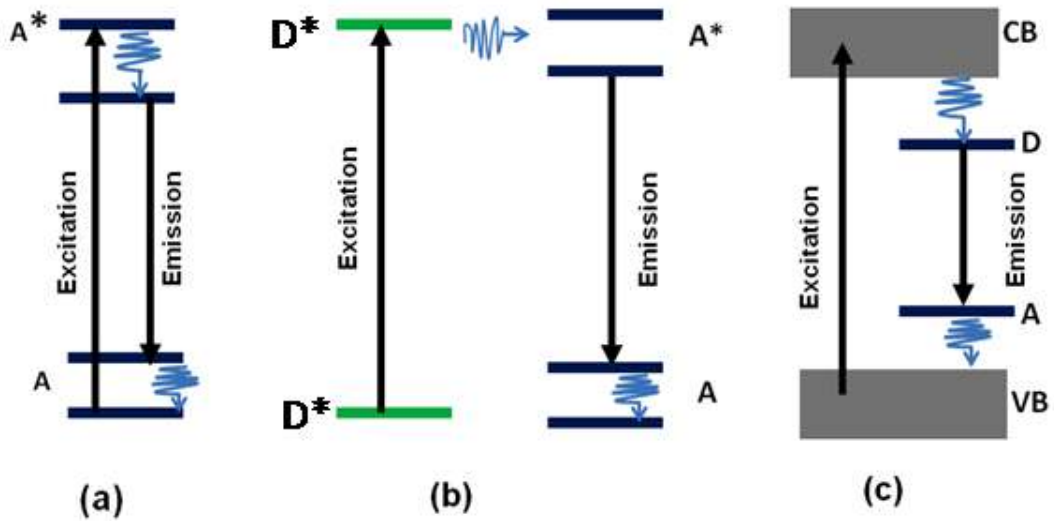

Figure 1.1: Schematic of the general luminescence mechanisms of phosphors: in localized center (a) and (b) and semiconductors (c).

The following sections describe the spectroscopy of RE ions in a solid matrix.

1.3 Rare-Earth Elements

RE elements or RE metals are a group of seventeen chemical elements in the periodic table (Figure 1.2), more precisely the fifteen lanthanides and two elements: scandium (Sc) and yttrium (Y). Scandium and yttrium are considered as RE elements because they exhibit similar chemical properties. Lanthanides are the series of elements from lanthanum (La, Z = 57) to lutetium (Lu, Z = 71). They adjust themselves at the

bottom of the periodic table, one row above the actinides. Lanthanide elements came into light after the discovery of the black mineral ytterbite (also known as gadolinite) by Lieutenant Karl Arrhenius in 1787, in a quarry in Ytterby village, Sweden.

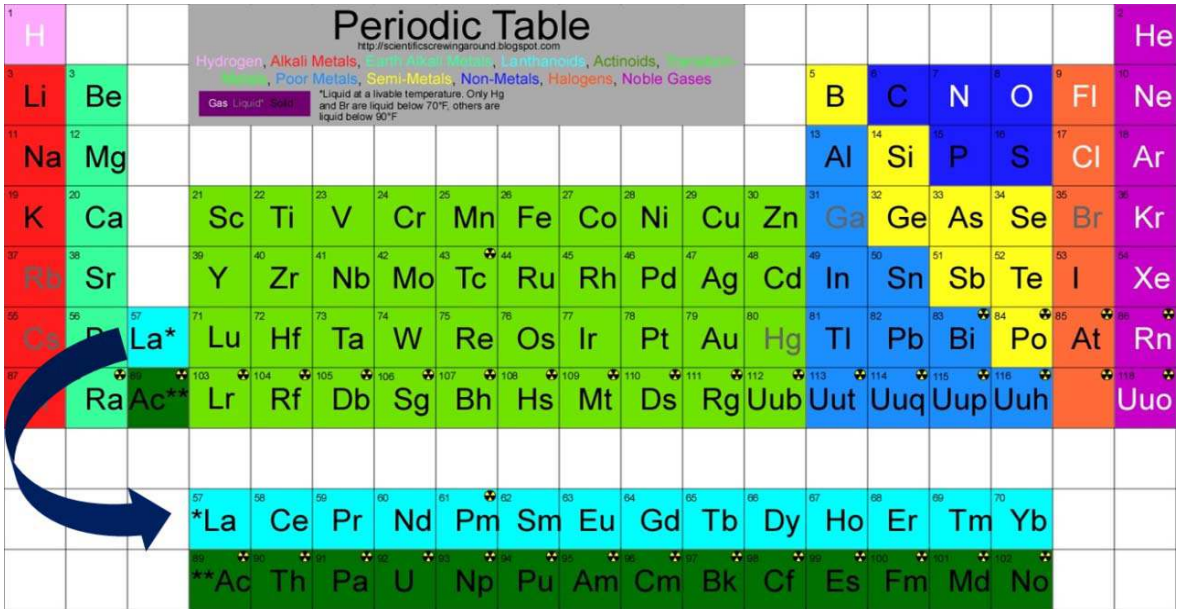

Figure 1.2: Periodic table of elements showing the position of lanthanides.

"Rare" word stands for the elements with a small quantity, while "Earth" is an obsolete term for oxide. It is taken from a French word "Terre". In correspondence to its geographical point of view, its name is a misnomer because its abundance is comparable to other elements such as silver, tungsten, and tin. Thulium (Tm), the least occurring lanthanide, is still more abundant than cadmium or silver. The lighter ions have higher abundance in these ores. They have a variety of technological importance such as in permanent magnets, catalysis, batteries, and optics [Jiang, et al. (1999)].

1.4 Characteristics of the Rare-Earth (Lanthanides) Elements

Rare-earth ions exhibit several distinct features in their chemistry that differentiate them from the d-block metals. Their reactivity is greater than that of the transition metals, similar to the group-II metals. Some of their properties are as follows:

- A substantial range of coordination numbers (6–12).
- Ligand steric factors determine the coordination geometries rather than crystal-field effects.
- RE ions form "ionic" complexes that undergo facile exchange of ligands.
- They exhibit small crystal-field splitting and very sharp electronic spectra as compared to the d-block metals.

- The 4f orbitals in the Ln^{3+} ion are well shielded by the $5s^2$ and $5p^6$ orbitals and do not participate directly in bonding. Their spectroscopic and magnetic properties are thus almost unaffected by the host.
- They prefer anionic ligands with donor atoms of high electronegativity (e.g., O & F).
- They readily form hydrated complexes (because of the high hydration energy of small Ln^{3+} ions), causing uncertainty in assigning coordination numbers.
- Insoluble hydroxides precipitate at neutral pH unless complexing agents are present.
- The chemistry is largely that of (3+) oxidation state (certainly in an aqueous solution).
- They do not form Ln=O or Ln≡N multiple bonds of the type known for many transition metals and certain actinides.
- Unlike the transition metals, they do not form stable carbonyls and have (virtually) no chemistry in the zero oxidation state.

Under a suitable environment, some RE elements also form other valence states such as 2+ and 4+.

1.5 Spectroscopy of Rare-Earth Elements

Rare-earth ions are characterized by a partially filled 4f shell that is shielded from external ligand fields by completely filled outer $5s^2$ and $5p^6$ shells. The energy levels of these elements are therefore largely insensitive to the environment in which they are accommodated. In general, the RE elements exist as 3+ or occasionally 2+ oxidation state when incorporated in crystalline or amorphous hosts. The 3+ ions exhibit intense narrow-band intra-4f luminescence in a wide variety of hosts, and the shielding provided by the $5s^2$ and $5p^6$ electrons leads to radiative transitions in solid hosts, resembling those of the free ions. Divalent RE species (e.g., Sm^{2+} and Eu^{2+}) also exhibit luminescence. This thesis mainly focuses on the luminescence of the trivalent RE ions.

Neutral RE elements have the electronic configuration (Xe) $4f^N6s^2$or (Xe) $4f^{N-1}$ 5d $6s^2$, where (Xe) represents a Xenon core, and the electronic structure of Xenon is [Xe] = $[1s^22s^22p^63s^23p^63d^{10}4s^24p^64d^{10}5s^25p^6]$. The ionization of the RE involves the removal of the two loosely bound 6s electrons, and then either a 4f or 5d electron (Table 1.1). The electrostatic shielding of the 4f electrons by the $5s^25p^6$ shells, similar to a metal sphere, is responsible for the atom-like properties of the lanthanides in a solid environment such as a crystal or glass. Table 1.1 shows the electronic configuration of RE ions, and a partial

energy-level diagram of the 4f–4f transitions of lanthanide ions is shown in Figure 1.3 (except for La and Lu).

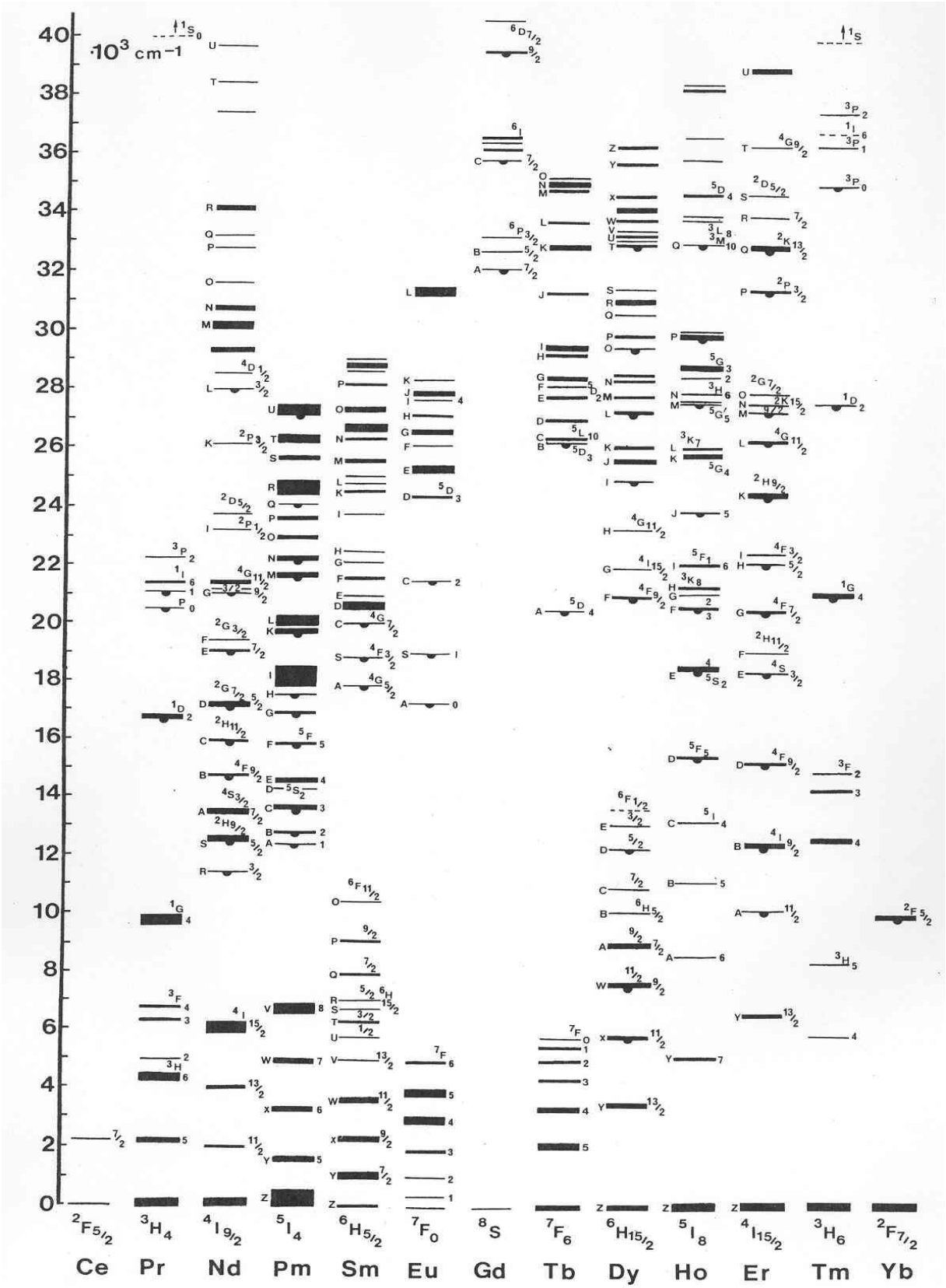

Figure 1.3: Partial 4f–4f energy-level diagram of Lanthanides [Dieke (1968)].

Table 1.1: Electronic configurations of atomic and trivalent ionic states of all the RE elements.

Atomic Number	Element	Atom electronic configuration	Ion electronic configuration	Color	Ground-state term
57	Lanthanum (La)	[Xe] $5d^1\ 6s^2$	[Xe] $4f^0$	Colorless	$^1S_0$
58	Cerium (Ce)	[Xe]$4f^2\ 5d^0\ 6s^2$	[Xe]$4f^1$	Colorless	$^2F_{5/2}$
59	Praseodymium (Pr)	[Xe]$4f^3\ 5d^0\ 6s^2$	[Xe]$4f^2$	Yellow green	$^3H_4$
60	Neodymium (Nd)	[Xe]$4f^4\ 5d^0\ 6s^2$	[Xe]$4f^3$	Lilac, violet blue	$^4I_{9/2}$
61	Promethium (Pm)	[Xe]$4f^5\ 5d^0\ 6s^2$	[Xe]$4f^4$	Pink, lilac	$^5I_4$
62	Samarium (Sm)	[Xe]$4f^6\ 5d^0\ 6s^2$	[Xe]$4f^5$	Pale yellow	$^6H_{5/2}$
63	Europium (Eu)	[Xe]$4f^7\ 5d^0\ 6s^2$	[Xe]$4f^6$	Colorless	$^7F_0$
64	Gadolinium (Gd)	[Xe]$4f^7\ 5d^1\ 6s^2$	[Xe]$4f^7$	Colorless	$^8S_{7/2}$
65	Terbium (Tb)	[Xe]$4f^9\ 5d^0\ 6s^2$	[Xe]$4f^8$	Colorless	$^7F_6$
66	Dysprosium (Dy)	[Xe]$4f^{10}\ 5d^0\ 6s^2$	[Xe]$4f^9$	Pale yellow	$^6H_{15/2}$
67	Holmium (Ho)	[Xe]$4f^{11}\ 5d^0\ 6s^2$	[Xe]$4f^{10}$	Yellow, Brownish pink	$^5I_8$
68	Erbium (Er)	[Xe]$4f^{12}\ 5d^0\ 6s^2$	[Xe]$4f^{11}$	Pink	$^4I_{15/2}$
69	Thulium (Tm)	[Xe]$4f^{13}\ 5d^0\ 6s^2$	[Xe]$4f^{12}$	Pale green	$^3H_6$
70	Ytterbium (Yb)	[Xe]$4f^{14}\ 5d^0\ 6s^2$	[Xe]$4f^{13}$	Colorless	$^2F_{7/2}$
71	Lutetium (Lu)	[Xe]$4f^{14}\ 5d^1\ 6s^2$	[Xe]$4f^{14}$	Colorless	$^1S_0$

This diagram is known as Dieke diagram [Carnall, et al. (1989)]. La^{3+} and Lu^{3+} have a completely empty and a completely filled 4f shell, respectively, and therefore have no optical transitions. Y^{3+} is usually also treated as a lanthanide ion, because of similar reactivity and coordination behavior. This ion also has no optical transitions, but luminescent RE ions are incorporated in Y_2O_3 host containing Y^{3+} ions. Ce^{3+} has one

electron and one 4f level just above the ground state. Ce^{3+} has the lowest oxidation potential of the RE ions, thus making the allowed 4f–5d transitions possible in the UV region.

The energy levels are denoted as $^{(2S+1)}L_J$ (Russell–Saunders notation as discussed in a later section), where S is the spin multiplicity, L the orbital angular momentum, and J the total angular momentum. In general, effective shielding of the 4f electrons eliminates the crystal-field effect; therefore, the energy-level diagram is identical for all sorts of host matrices. Table 1.2 shows some RE transitions that are used in devices or have potential for particular application.

Table 1.2: Some of the important transitions of the RE ions and their applications.

Ion	Transition	Wavelength (nm)	Applications
Pr^{3+}	$^1G_4 \rightarrow {}^3H_5$	1300	Optical amplifier
Nd^{3+}	$^4F_{3/2} \rightarrow {}^4I_{11/2}$	1064	Solid-state lasers
Eu^{3+}	$^5D_0 \rightarrow {}^7F_2$	615	Displays, lighting
Tb^{3+}	$^5D_4 \rightarrow {}^7F_5$	545	Displays, lighting
Dy^{3+}	$^6F_{11/2} + {}^6H_{9/2} \rightarrow {}^6H_{15/2}$	1300	Optical amplifier
Er^{3+}	$^4I_{13/2} \rightarrow {}^4I_{15/2}$ $^4S_{3/2} \rightarrow {}^4I_{15/2}$ $^2H_{11/2} \rightarrow {}^4I_{15/2}$	1530 550 525	Optical amplifier, Upconversion laser [Finger printing, Display devices, Optical temperature sensors]
Tm^{3+}	$^1G_4 \rightarrow {}^3H_6$ $^3F_4 \rightarrow {}^3H_4$	488 1480	Upconversion display Optical amplifier,
Yb^{3+}	$^2F_{5/2} \rightarrow {}^2F_{7/2}$	980	Sensitizer, solid-state NIR laser

1.6 Rare-Earth Ion Levels in Solids

A notable feature of the RE ions doped into crystals is the large number of sharp lines in their absorption and emission spectra ranging from UV–visible to IR. This results from their intraconfigurational transitions (4f–4f). The 4f–4f transitions are forbidden according to Laporte rule and have very weak oscillator strength of the order 10^{-6}. The RE ions in bulk materials has a perturbative effect that shifts and splits the free-ion energy levels. These perturbed electronic states can also interact with the phonon states of the crystal lattice, producing various effects. Considering the importance of the issues related

with the origin of the transitions, some fundamental aspects of the RE energy levels are discussed below:

The $4f^N$ configuration of a RE ion produces several electronic states. The spread of $4f^N$ energy levels arises from the various atomic interactions between electrons and can be obtained by solving the time-dependent Schrodinger equation. From the weak interaction of the 4*f* electrons with the electrons from other ions and host lattice, the Hamiltonian of an individual RE ion can be expressed as follows [Miniscalco (2001)]:

$$H = H_{free\ ion} + V_{Host} + V_{EM} + V_{Vibrational} + V_{ion–ion} \quad (1.1)$$

where $H_{free\ ion}$ is the Hamiltonian of an isolated ion, V_{Host} describes the effect of the environment on the RE ion, V_{EM} describes the interaction of RE ion with an electromagnetic field, $V_{Vibrational}$ describes the interaction of RE ion with the vibrations of the host lattice, and $V_{ion–ion}$ describes the interaction between the RE ions.

The Hamiltonian of free ion ($H_{free\ ion}$) can itself be broken into several components,

$$\text{i.e.,} \quad H_{free\ ion} = H_{CF} + H_C + H_{SO} \quad (1.2)$$

where H_{CF} is the central-field Hamiltonian, which describes the interaction of an orbiting electron with the nucleus and effective centrally symmetric field from all other electrons. The H_c term describes the residual Coulomb interaction of the 4*f* electrons with each other once the centrally symmetric contribution is removed, and H_{SO} is the spin–orbit coupling term.

The interaction terms other than $H_{free\ ion}$ in Eq. (1.1) are comparatively weak for treating as separate perturbations. The terms $H_{free\ ion}$ and V_{Host} are static interactions and produce the observed electronic states of the RE ion, while V_{EM}, $V_{Vibrational}$, and $V_{ion–ion}$ are dynamic perturbations and result in transitions between the states established by the static interactions. The term H_{CF} in the free-ion Hamiltonian causes a splitting of the $4f^n$ electronic state into several states with different energies, characterized by the angular and spin quantum numbers *L* and *S*. In the case of RE atoms with large atomic numbers, spin–orbit coupling is significant, and the states are eigenstates of *J*, but not of *S* or *L*. The spin–orbit interaction eliminates the degeneracy in the total angular momentum ($J = L + S$). Russell–Saunders coupling (LS coupling) is consistently used to describe the states of the lanthanides. In this scheme, *L* and *S* are vectorially added to form the total angular momentum *J*, and the states are labeled as $^{2S+1}L_J$. The term H_{SO} represents the spin–orbit coupling of the LS states, and results in a further splitting of the LS terms into *J* levels. The magnitudes of the spin–orbit coupling and residual Coulomb splitting can be of the

same order, which results in L and S not always being good quantum numbers and the eigenstates of the system being a superposition of the Russell–Saunders (LS) states, a situation known as intermediate coupling [Hufner (1978)]. Because of this mixing of states, some confusions arise, e.g., in the case of Tm^{3+}, the energy manifolds can either be labeled according to their dominant LS contribution, as experimentally observed, or agree with the zero spin–orbit convention. If LS contribution dominates, the energies of the $^3F_4$ and $^3H_4$ levels would be at 6000 and 12500 cm^{-1}, respectively, while the zero spin–orbit convention would label these states at the same positions as $^3H_4$ and $^3F_4$, respectively.

In general, the shielding of 4f electrons by the electrons of the 5s, 5p, and 6s orbitals causes only slight splitting of the $^{2S+1}L_J$ levels, and the magnitude of the splitting can be derived from crystal-field theory [Inoue, et al. (2002)]. The crystal-field potential at the ion site can be described in terms of a power series of tensor operator components given by Wybourne (1965):

$$V_{site} = \sum_{ikq} B_q^k [C_q^k] i \tag{1.3}$$

where the summation over i involves all the 4f electrons of the ion. B_q^k is the radially dependent part of the one-electron crystal-field interaction consisting of the coefficients of expansion, known as crystal-field parameters ($k \leq 6$ for f electrons). B_q^k is a function of electron density with a parametric dependence on the lattice structure and can be evaluated empirically from the experimental data. C_q^k are the many-electron spherical tensor operators for the $4f^n$ configuration. The even k terms in the expansion split the free-ion J multiplets into Stark components, generally separated by 10–100 cm^{-1}. This follows from the triangle rule for the addition of angular momentum $l_1 + l_2 \geq k$. The values for k and q are also limited by the point symmetry of the ion as the Hamiltonian must be invariant under the operations of the point-symmetry group. The applicable values of "q" depend on the site symmetry of the lanthanide ion in the host lattice. The odd k terms admix the higher lying states of opposite parity into the $4f^n$ configuration. This admixture does not affect the position of the energy levels, but significantly affects the strengths of the optical transitions between the levels [Miniscalco (2001)].

The crystal-field splitting is a function of the symmetry of the ion and the resultant magnitude of the field. The knowledge of the symmetry at the site of the ion can be used to predict the number of levels in a given J state.

Table 1.3: J splitting under various point symmetries.

J	0	1	2	3	4	5	6	7	8
Cubic	1	1	2	3	4	4	6	6	7
Hexagonal	1	2	3	5	6	7	9	10	11
Tetragonal	1	2	4	5	7	8	10	11	13
Lower symmetry	1	3	5	7	9	11	13	15	17

The number of levels of a state of angular momentum J splits for a given point symmetry is shown in Table 1.3. RE ions can be used to probe the crystal symmetry by knowing the number of J splitting of the levels. The actual position of the energy level and splitting is determined by the resultant Hamiltonian described in Eq. (1.1). The splitting of the $4f^n$ configuration of Eu^{3+} ion is shown in Figure 1.4. The electrostatic interaction or Coulomb repulsion splits ^{2S+1}L of the order of 10^4 cm^{-1}. The spin–orbit interaction splits the levels further into $^{2S+1}L_J$, separating the J states by 10^3 cm^{-1}. Finally, the crystal field removes the degeneracy in J with an energy-level separation of the order 10^2 cm^{-1}. The extent to which the Stark sublevels spread depends on the strength of the crystal field. The larger the crystal field, the larger the spread of the J sublevels. It is expected that several mechanisms may operate to observe the forbidden electric dipole transitions, which are small but have significant amplitude. The applicable selection rules in RE ions are shown in Table 1.4.

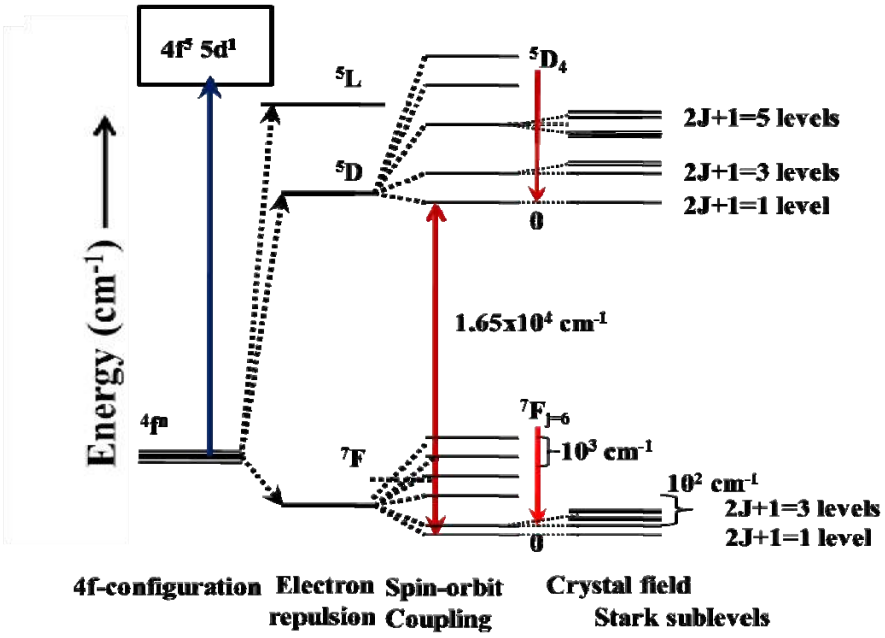

Figure 1.4: Splitting of the Eu^{3+} ion energy levels under various perturbations.

Table 1.4: Selection rules for f–f transitions in rare-earth ions.

Operator	**Parity**	**ΔS**	**ΔL**	**ΔJ***
Electric dipole	Opposite	0	≤6	≤6 (2, 4, 6, if J or J′ = 0)
Magnetic dipole	Same	0	0	0, ±1
Electric quadrupole	Same	0	0, ±1, ±2	0, ±1, ±2
* J = 0 to J′ = 0 transitions are always forbidden J = 0 → J′ = 1, 3, 5 are weak J = 0 → J′ = 2, 4, 6 are strong				

Although the shielding of the 4f electrons makes them insensitive towards the proximate field, a few transitions exaggerate the small changes in the lattice coordination sphere. These transitions are termed as *hypersensitive* transitions. Jorgenson and Judd [Jorgensen (1971)] observed that hypersensitive transitions obey the selection rules $\Delta J \leq 2$, $\Delta L \leq 2$, and $\Delta S = 0$. Moreover, these are the selection rules for quadrupole transitions. The hypersensitive transitions do not have a quadrupolar character. Some important hypersensitive transitions observed in the lanthanide ions are shown in Table 1.5.

Table 1.5: Hypersensitive transitions observed in rare-earth ions.

RE ion	**Transition**	**Energy (cm^{-1})**	**Wavelength (nm)**
Pr^{3+}	$^3F_2 \rightarrow {}^3H_4$; $^3P_2 \rightarrow {}^3H_4$	5200, 22207	1923, 450
Nd^{3+}	$^4G_{5/2} \rightarrow {}^4I_{9/2}$	17300	578
Sm^{3+}	$^6F_{1/2,3/2} \rightarrow {}^6H_{5/2}$	6397	1563
Eu^{3+}	$^5D_0 \rightarrow {}^7F_2$, $^5D_2 \rightarrow {}^7F_0$, $^5D_1 \rightarrow {}^7F_1$	16308, 21500, 18700	613, 465, 535
Dy^{3+}	$^6F_{11/2} \rightarrow {}^6H_{15/2}$	7663	1305
Ho^{3+}	$^5G_6 \rightarrow {}^5I_8$; $^3H_6 \rightarrow {}^5I_8$	22100, 27700	452, 361
Er^{3+}	$^4G_{11/2} \rightarrow {}^4I_{15/2}$	26400	379
Tm^{3+}	$^3F_4 \rightarrow {}^3H_6$; $^3H_4 \rightarrow {}^3H_6$	12000, 5900	833, 1664

In the case of hypersensitive transitions, the value of square reduced matrix element $\left\|U^{\lambda}\right\|^2$ is large compared to the values for other transitions. The intensities of the hypersensitive transitions have also been correlated with the site symmetry of the RE ions. The intensity is found to strongly decrease in higher symmetric sites. Hypersensitivity of a

transition has been shown to be directly proportional to the nephelauxetic ratio, which is a measure of the covalancy of the R–O bond [Jorgensen (1971)].

1.7 Hosts for Rare-Earth Ion

The choice of host materials is of great importance in designing lanthanide-based luminescent materials for efficient device applications. As a general rule, the host materials require close lattice matches to the dopant ions and have low phonon frequencies. Despite the fact that the energy-level structure of most lanthanide ions is independent of the host materials, phonon energy plays an important role in nonradiative transitions due to multiphonon relaxation between closely spaced energy levels. The nonradiative relaxation rate can be estimated using the exponential energy gap law:

$$k_{nr}=\beta_{el}exp(-\alpha(\Delta E-2\hbar\omega_{max})) \quad (1.4)$$

where β_{el} and α are constants for a given host lattice, ΔE is the energy difference between the energy levels considered, and $\hbar\omega_{max}$ is the maximum phonon energy. Hosts with low phonon energy may decrease the probability of nonradiative transitions, subsequently leading to a high luminescence efficiency.

A list of cut-off phonon frequencies of some of the phosphors and glass host matrices are shown in Table 1.6.

Table 1.6: Energy of the maximum phonon frequency for different hosts [Yen, et al. (2006)]

Materials	**Phonon Vibration (~ħω cm^{-1})**
Borate	1400
Phosphate	1100
Silicate	1000–1100
Germanate	800–975
$CaMoO_4$	800
$Y_2TI_2O_7$	712
Tellurite	600–850
Y_2O_3	550
YVO_4	600
Fluoride	500–600
$LaCl_3$	260
Bromide	175–190
$LaBr_3$	175
Iodide	160

1.7.1 Fluoride based host for display and bio applications

The tremendous recent advances in nano technology have led to the development of new types of probes based on nano-particles. Upconversion nanoparticles (UCNPs) have been developed as a new class of fluorescence bioprobes and as promising alternatives to conventional organic dyes and semiconductor quantum dots luminescence labels, due to the many attractive merits such as high quantum yields, narrow emission peak, long lifetimes, large Stokes shifts, superior photostability, and low toxicity [Auzel (2004), Feldmann, et al. (2003)]. In particular, UCNPs for both in vitro and invivo optical bio-imaging application holds such advantages as absence of pho-todamage to live organisms, very low autofluorescence background, high signal-to-noise ratio and detection sensitivity, and high light penetration depth in biological tissues [Xiong, et al.(2009)]. In addition, IR light with strong penetration ability is safe to the human body and less harmful to cells [Chatterji, et al. (2008)]. Moreover, multiplexed biological labelling can be achieved conveniently by changing different activator ions and concentrations under the single-wavelength excitation, which can extend their capabilities for simultaneous imaging and tracking of multiple molecular targets, e.g. allowing scientists to understand, classify and differentiate complex human diseases [Li, et al.(2008)]. To date, Yb/Er (orYb/Tm) co-doped $NaYF_4$ nanocrystals have been reported as the most efficient NIR-to-visible up-conversion material known. Especially β-$NaYF_4$:Yb^{3+}, Er^{3+} UCNPs have been used for the detection of DNA, avidin and immune labeling [Li and Lin (2010), Heer, et al.(2003), Wang and Li (2006)].

It is worth pointing out that the crystal phase, size and shape of fluorides have important effect on their emission properties. For $NaREF_4$, hexagonal phase nanocrystals have higher luminescence efficiency than cubic-phase nanocrystals due to more ordered structure and multisite character in the hexagonal form. Recently, Ghosh and Patra investigated the influence of crystal phase on luminescence properties of Eu^{3+}-doped $NaYF_4$ nanocrystals [Ghosh and Patra (2008a), Ghosh and Patra (2008b)]. They investigated the influence of crystal phase and excitation wavelength on luminescence properties of $NaYF_4$: Eu^{3+} nanocrystals. Veggel and his co-worker reported fluorides based composites show brilliant emission intensity and can be used in display devices [Shivakumar, et al.(2005), Sudarsan, et al.(2005), Shivakumar, et al.(2009)]. Also these fluoride based nanomaterials are used in photodianmic therapy, contrast agent in MRI, and carriers in a drug delivery [Li and Lin (2010)].

1.7.2 Pyrochlore based Phosphors

Among the up-conversion phosphor materials, pyrochlore titanates $Y_2Ti_2O_7$ (YTO) has attracted attention due to its thermal stability, low phonon energy (~ 712 cm^{-1}), photo-catalytic behaviour and high refractive index value (~2.34) [Dai, et al. (2012), Fuentes, et al. (2005), Abe, et al. (2006), Ting, et al, (2011)]. The optical band gap of host material $Y_2Ti_2O_7$ is ~3.7 eV. This wide band gap of the host reduces a quenching effect on the emission of Ln^{3+} ion [Ting, et al.(2011), Chen, et al.(2012)]. In $Y_2Ti_2O_7$, there are four different crystallographic axes, namely, Y(16d), Ti(16c) ,O1(48f), and O2(8b) assuming that aTi^{4+} ion is situated at the origin of the unit cell. The Y and Ti sites have eight and six ion co-ordination sites, respectively, while the crystallographically different axis of oxygen O1 (48f) was co-ordinated to 2Ti and 2Y. O2(8b) was co-ordinated to 4Y ions, while the third anionic site,O3(8a), was co-ordinated to the 4Ti ions and generally found to be empty in the ordered pyrochlore lattice shown in Figure 1.5 [Subramanian, et al.(1983), Mandal, et al.(2011)]. Wang, et al.(2012) reported the upconversion behavior of Er^{3+}/Yb^{3+} doped $Y_2Ti_2O_7$ and the pump power saturation mechanisms and dominant red band over green was observed. Yan, et al.(2012) reported on $Y_2Ti_2O_7$: Yb^{3+}, Er^{3+}, Tm^{3+} upconversion inverse opal photonic crystals with energy transfer between Er^{3+} and Tm^{3+}. They have investigated the influence of the photonic band gap on the energy transfer between Tm^{3+} and Er^{3+}. Furthermore result showed that strong modification of the steady state upconversion emission spectra was observed, and the green or red upconversion emission from Er^{3+} was suppressed in the inverse opal.

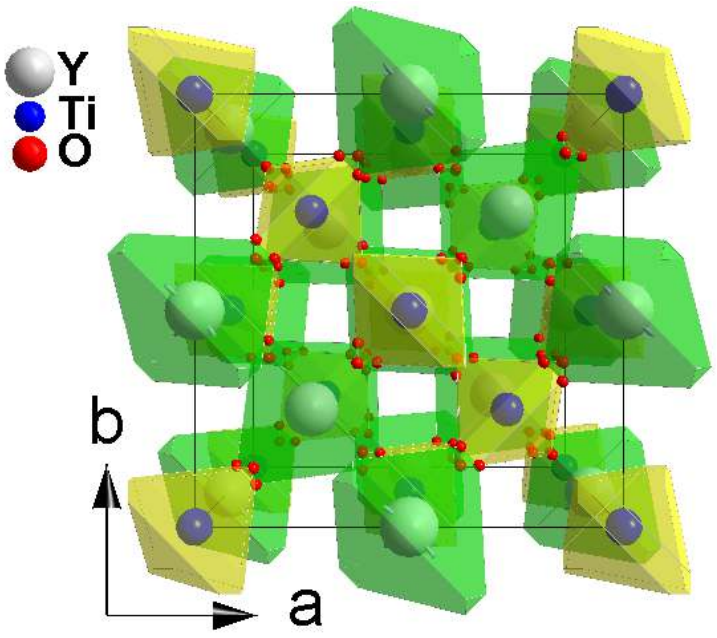

Figure 1.5: Schematic illustrating the crystal structure of tetragonal $Y_2Ti_2O_7$.

More significantly, the energy transfer between Tm^{3+} and Er^{3+} is enhanced by suppression of the red upconversion emission of Er^{3+}, thus the blue upconversion emission from Tm^{3+} is considerably improved in the inverse opals. Additionally, the mechanisms for upconversion emission of the $Y_2Ti_2O_7$: Yb^{3+}, Er^{3+}, Tm^{3+} inverse opal are discussed. Results corroborated the utility of upconversion emission modification and the application of upconversion displays and short wavelength upconversion lasers. Pavitra, et al.(2012) reported the optical properties of Eu^{3+} doped $Y_2Ti_2O_7$ prepared via solvothermal process. Crystallinity appears at 800 ^oC annealed samples. Result showed its potentiality in display devices.

1.7.3 Scheelite type Molybdate Phosphors

Nano-and microcrystals doped with lanthanide ions play an important role in modern lighting and display field due to their unique optical and chemical properties. Contrary to conventional luminescent materials (such as organic fluorescent dyes or semiconductor quantum dots) lanthanide doped materials show narrow emission bands, longer luminescence lifetimes and low photo-bleaching [Gupta et al.(2009)] Rare earth tungstates and molybdates have been proved to be good host lattices for the luminescence of lanthanide ions. They show good chemical and thermal stability. Undoped rare earth molybdates emit blue-green light under ultraviolet excitation. The photoluminescence properties of various lanthanide doped nano-and micro structured rare earth tungstates and molybdates have been investigated in detail by researchers [Cavalcante, et al.(2012), Longo, et al.(2011)].

It is well known that scheelite-type ABO_4 (A = alkali metal, Ca^{2+}, Sr^{2+}, Ba^{2+}, Bi^{3+}, B = Mo^{6+}, W^{6+}) compounds are important functional materials in the field of scintillation detectors, phosphors, lasers, photo-catalysts and lithium-ion batteries [Cavalcante, et al.(2012), Longo, et al.(2011), Guo, et al. (2014)]. $CaMoO_4$ has a tetragonal unit cell with space-group symmetry $I4_1/a$. Parchur, et al.(2011(a), 2012(a)) reported the luminescent properties of Eu^{3+} and Tb^{3+} doped $CaMoO_4$ nanophosphors via polyol synthesis. Nanoparticles are prepared by using polyol method under urea hydrolysis at low temperature (~120-150 ^oC). Their structural and luminescence properties of these have been studied. Different particle sizes and annealing effects are investigated. As the particle size decreases emission intensity decreases significantly due to multi phonon relaxation process. These nanoparticles are suitable for various optoelectronic and biomedical applications, like medical diagnostics, imaging in confocal microscopy,

display devices, and optical fiber communication. The advantage with $CaMoO_4$ as a host material is that it has high melting point, high refractive index and non-hygroscopic. Further, it has low phonon frequency (~800 cm^{-1}), which reduce the probability of multi phonon relaxation process between the rare earth ions electronic levels. Raghumani and his co-workers also reported the bi-functional properties of $CaMoO_4$:Eu@$CaMoO_4$ core shell formation. They have reported the enhanced luminescent properties after core-shell formation. Result shows that this compound has been used as hyperthermia applications as well as bio-imaging [Parchur, et al.(2014)]. The A-site cation is coordinated by 8 oxygen anions by relatively weak forces, and the B-site cation is surrounded by 4 oxygen anions forming a tightly bound BO_4 tetrahedron, as shown in Figure 1.6.

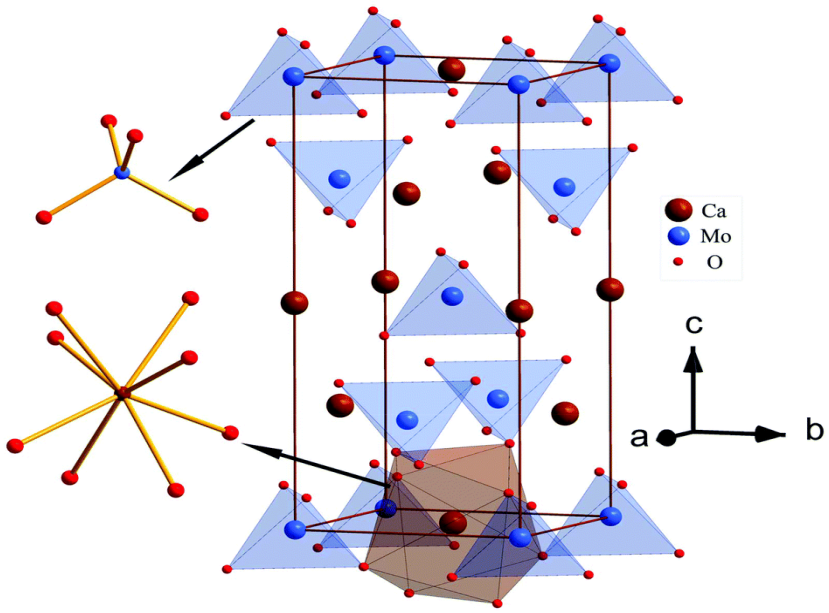

Figure 1.6: Schematic illustrating the crystal structure of tetragonal $CaMoO_4$.

1.8 Physical Properties of Rare-Earth-Doped Materials

From the measured refractive index (n) and density (d) of the rare-earth-doped materials, several physical parameters can be calculated using different relations [Kumar (2008)]:

➢ RE ion concentration

The RE ion concentration N in the sample can be calculated from the density (d) and average molecular weight of the sample ($\overline{M}$):

$$N = \frac{N_A(M\%RE)d}{\overline{M}} \tag{1.4}$$

where N_A is the Avogadro's number.

- **Ionic radius**

The ionic radius (r_P) is determined from the value of ion concentration (N) as follows**:**

$$r_p(A^0) = \frac{1}{2}\left(\frac{\pi}{6N}\right)^{1/3} \tag{1.5}$$

- **Mean atomic volume**

The mean atomic volume can be calculated as follows:

$$\mathrm{V\ (cm^3\ atom^{-1})} = \frac{\overline{M}}{(Total\ \ No.\ of\ atoms)d} \tag{1.6}$$

- **Electronic polarizability**

The molecular electronic polarizability is determined using the Clausius Mossotti equation as follows:

$$\alpha_e\left(cm^3\right) = \frac{(n-1)/(n^2+2)}{(4\pi/3)(d.N_A/\overline{M})} \tag{1.7}$$

- **Molecular refractivity**

The molecular refractivity is estimated from the following relation:

$$R_M(Cm^3) = \frac{(n^2-1)\overline{M}}{(n^2+2)d} \tag{1.8}$$

- **Field strength**

The electric field strength created by a RE ion in a sample is determined by the following relation:

$$\mathrm{F\ (cm^{-2})} = \frac{Z}{r_p^{\ 2}} \tag{1.9}$$

- **Reflection losses**:

Reflection losses from the sample surface can be calculated from the Fresnel's formula:

$$\mathrm{R\%} = \frac{(n-1)}{(n+1)} \times 100 \tag{1.10}$$

1.9 Judd–Ofelt Theory

This theory is used to calculate various optical parameters of RE-doped materials based on their absorption and fluorescence spectra. The absorption spectra of free RE ions show relatively sharp lines arising from 4f–4f electronic transitions, which can be induced electric dipole, magnetic dipole, or electric quadrupole in character. A quantitative treatment for the intensities of these transitions has been developed independently by Judd (1962) and Ofelt (1962). For a free RE ion, the electric dipole transition between

two states with 4f configuration is parity forbidden, while the magnetic dipole and electric quadrupole transitions are allowed. For an ion in a host medium, electric dipole transitions are also allowed due to the admixture of states from the configurations of opposite parity (for example, mixing of $4f^{n-1}$ 5d with $4f^n$ configuration). The transition probability depends on the extent of this admixture. Judd–Ofelt theory needs the measurement of absorption spectrum for calculating Judd–Ofelt intensity parameters. Fluorescence spectrum can be used to calculate the radiative properties of the fluorescing levels of a particular RE ion.

(A) Absorption spectra

The intensity of an absorption band is expressed in terms of oscillator strength. According to the model, the oscillator strength of a transition between an initial J manifold (S, L, and J) and a final J′ manifold (S′, L′, and J′) can be expressed as follows:

$$F_{cal}\,(aJ, bJ') = \frac{8\pi^2 m\upsilon}{3h(2J+1)}\left[\left\{\frac{(n^2+2)^2}{9n}\right\}S_{ed} + nS_{md}\right] \tag{1.11}$$

$$\text{where, } S_{ed}\,[(S, L, J); (S', L', J')] = \sum_{\lambda=2,4,6}\Omega_\lambda\left|\left\langle (S, L, J)\right\|U^\lambda\left\|(S', L', J')\right\rangle\right|^2$$

$$\text{and } S_{md}\,[(S, L, J); (S', L', J')] = \sum_{\lambda=2,4,6}\Omega_\lambda\left|\left\langle (S, L, J)\right\|L + 2S\left\|(S', L', J')\right\rangle\right|^2$$

Here, S_{ed} and S_{md} represent the line strengths corresponding to the induced electric and magnetic dipole transitions, respectively. The three intensity parameters Ω_λ (λ = 2, 4, and 6) are known as *phenomenological Judd–Ofelt intensity parameters*. They depend upon their interconfigurational radial integrals, the energy separation between the levels, and the configuration of opposite parity. These parameters are sensitive to the structural changes. The term $\|U^\lambda\|$ represents the matrix elements of the unit tensor operator U^λ related to the initial and final states of the transition and shows slight dependence on host.

Experimentally, it is expressed by the area under the absorption band [Carnell, et al. (1963)]

$$f_{meas} = \frac{mc^2}{\pi e^2 N}\int\frac{\alpha(\lambda)d\lambda}{\lambda^2} \tag{1.12}$$

where $\alpha(\lambda) = 2.303\times OD(\lambda)/d$ is the measured absorption coefficient at a given wavelength λ, OD (λ) is the optical density, i.e., [log I/I_0] as a function of wavelength λ, d

is the thickness of the sample, m and e are the mass and charge of the electron, respectively, c is the velocity of light, and N is the number of RE ions per unit volume. The absorption bands in glasses are relatively broad because of the disorder and are generally not purely Gaussian in shape. However, it is usually a good approximation to use a Gaussian error curve [Jorgensen (1962)] to represent the absorption profile.

$$\varepsilon = \varepsilon_{\max} \; 2^{-\frac{(\nu-\nu_0)^2}{\Delta\nu_{1/2}^2}} \tag{1.13}$$

$$\varepsilon_{\max} = \frac{OD(\nu)}{d * N}$$

υ_0 is the frequency of the absorption band where the molar extinction coefficient ε is the maximum. $\Delta\upsilon_{1/2}$ is the half width at half maximum (in cm^{-1}). Oscillator strength can be expressed as follows:

$$f_{meas} = 2.303 \frac{mc^2}{\pi e^2 N} 2.1289 \varepsilon_{\max} \Delta\upsilon_{1/2} \tag{1.14}$$

According to the Judd–Ofelt theory, the theoretically calculated and experimentally observed oscillator strengths should be equal. The parameters Ω_λ can then be estimated through a least-squares fitting of the experimental results. The same parameters are then used to calculate the electric dipole contribution to the total spontaneous emission probabilities.

(B) Fluorescence spectra

The Judd–Ofelt parameters obtained from the absorption measurements are used to describe the radiative properties of the fluorescing levels. The spontaneous emission probability for an electric dipole (allowed) transition may be obtained from the expression [Rotenberg, et al. (1959), Nielson, et al. (1964), Weber, et al. (1981)]

$$A(\psi'_{J'} \rightarrow \psi_J) = \frac{64\pi^2\nu^3}{3h(2J+1)} \frac{n(n^2+1)^2}{9} S_{ed} \tag{1.15}$$

The relaxation rate (total transition probability) from an initial manifold J′ to a final manifold J can be expressed as follows:

$$A_J = \sum_J A(\psi'_{J'} \rightarrow \psi_J) \tag{1.16}$$

The radiative lifetime (τ_t) of the fluorescing level is given as follows:

$$\tau_t = \frac{1}{\sum_J Aj} \tag{1.17}$$

The fluorescence branching ratio β_R is obtained from [Hufner (1978)]

$$\beta_R(\psi'_{J'}) = \frac{A(\psi'_{J'} \rightarrow \psi_J)}{\sum_J A(\psi'_{J'} \rightarrow \psi_J)} \tag{1.18}$$

Finally, the stimulated emission cross-section for the transition from J′ to J is given as follows:

$$\sigma = \frac{\lambda^4}{8\pi^2 c n^2 \Delta\lambda} A(\psi'_{J'} \rightarrow \psi_J) \tag{1.19}$$

where λ is the wavelength of the spectral line, and Δ λ is the effective band width, which is used because of the asymmetry of the bands and is obtained by dividing the integrated intensity of the emission band by the intensity at the peak of the band.

1.10 Upconversion Fluorescence

Upconversion is a process in which incident light of lower frequency is converted into output light of higher frequency by interacting with a suitable atomic/molecular system. The light upconversion process has applications in photonic devices, biomedical diagnostics, temperature sensors, upconversion lasers, infrared laser viewers, and indicators etc. Before the 1960s, all the observed anti-Stokes emissions involved emission energies in excess of the excitation energies by only a few kT. They were linked to the thermal population in the energy levels above the ground state. Therefore, thermoluminescence can also yield anti-Stokes emission. Superexcitation, i.e., excitation of an already excited state by the absorption of an incident photon (excited-state absorption, ESA) was also known, but resulted in very weak anti-Stokes emissions. Reviews of such well-known anti-Stokes processes have been documented in literature. [Auzel(1990)]. Lanthanide ions with possible transitions between the levels of intraconfigurational 4f shell often have long lifetimes and thus may produce upconversion emissions of the anti-Stokes type under moderate-to-strong incident excitation. Several different mechanisms have been identified for upconversion either in singly doped or codoped samples.

1.10.1 Excited-state absorption (ESA)

The principle of ESA was proposed in 1959 by Bloembergen with the idea of constructing a solid-state counter for IR or millimeter wave quanta. Since that time, this technique of successive photon absorptions by the same ion (Figure 1.7) has been used to generate fluorescence at a higher frequency than that of the incident radiation.

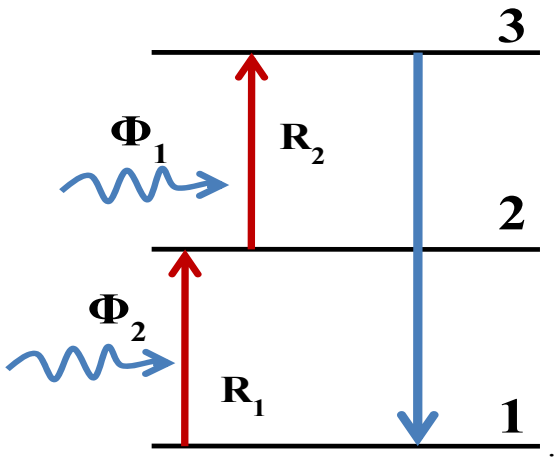

Figure 1.7: General energy scheme related to the ESA.

For photons of the incident flux Φ_1 with energy resonant with the transition energy between ground state 1 and excited state 2, some of these incident photons would be absorbed under the ESA process; an ion excited to state 2 absorbs a fresh incident photon to get excited to level 3. Thus, ions are excited to a much higher excited state than normally possible for the given incident frequency. ESA is a single-ion process and is independent of the RE ion concentration in the material. Under continuous wave (CW) excitation, provided there is no saturation of state 2, the anti-Stokes (from level 3) fluorescence is almost proportional to the product $\Phi_1\Phi_2$ of the incident photon fluxes. In the particular case, when two transitions $1 \rightarrow 2$ and $2 \rightarrow 3$ have the same energy, only one excitation beam (Φ) is necessary, and the anti-Stokes fluorescence is almost proportional to Φ^2 [Guy, et al. (1993)]. A more general, if *n* successive absorptions are required, the anti-Stokes fluorescence is almost proportional to Φ^n. The anti-Stokes fluorescence decay measured under short-pulsed laser excitation characterizes only the relaxations of state 3; thus, it is identical to that measured after the direct excitation of state 3.

Looking at the ESA mechanism as an upconversion laser pumping process, it appears that, for most of the RE-doped crystals, it would be necessary to use two pump laser beams, one resonant with the ground-state absorption transition and the other resonant with the ESA transition. This disadvantage may be ruled out if there is perfect coincidence between these two transition energies, where the energy mismatch is compensated by the absorption or emission of phonons, when the transitions are broadened by inhomogeneities as it is the case in disordered materials.

Moreover, as ESA is a single-ion process, the ideal would be a low active ion concentration to avoid transfer losses.

1.10.2 Energy-transfer upconversion (ETU)

Until the mid-1960s, all energy transfers (ETs) between two RE ions were of the type where the sensitizer (or donor) ion is in one of its excited states, while the activator (or acceptor) ion is in its ground state; and the interaction transfers the excitation energy (or a part of it) from the donor to the accepter ion. This process explained sensitized fluorescence and concentration quenching.

In 1966, it was proposed that this type of ET which excites the acceptor ion to one of its excited states may be followed by the absorption of an additional pump photon, promoting the acceptor ion into a still higher excited state [Auzel (1976, 2004)]. Moreover, an ET can occur from the sensitizer to an activator ion, which is already in one of its excited states. Both these mechanisms would lead to possible fluorescence at a higher frequency than the incident frequency. Such ET upconversions (ETU) have been reported in materials codoped with two types of RE ions, e.g., Yb^{3+}/Er^{3+} and Yb^{3+}/Tm^{3+}, and used to obtain more efficient IR quantum counters. The different types of ETU processes are shown schematically in Figure 1.8.

The cases A, B, and C of Figure 1.8 do not involve any cooperative effect. The first case (Figure 1.8 A) is the conventional ET upconversion in which the sensitizer in its excited state transfers its excitation energy to the ground state of activator, and the excited activator absorbs a second input photon and excited to a higher excited state 3. The second case (Figure 1.8 B) involves successive ET from the sensitizer to the activator raising the latter to a high-energy excited state. This is the process of choice when only the sensitizer can absorb photon from the incident beam. Figure 1.8 (C) shows a process, which may be termed as cross-relaxation upconversion (CRU). Indeed, in this case, the two ions involved in ET are identical, and both of them are excited to an excited state by absorbing incident photons. One of these ions relaxes to the ground state, and the released excitation energy raises the second ion to a much higher excited state.

When more than one ion takes part in the sensitization process, cooperative effect occurs. Figure 1.8 (D) shows the process. In this case, the energy accumulated by two excited ions is transferred to one ion, which reaches a high excited state. Figure 1.8 (E) shows the cooperative upconversion phenomenon. In this process, two ions are excited by the incident radiation to an excited level. Two excited ions combine their energies in such a way that one ion emits the sum of the energies. For all these processes, anti-Stokes emission intensity I is directly proportional to the product $\Phi_1\Phi_2$ of the incident photon fluxes.

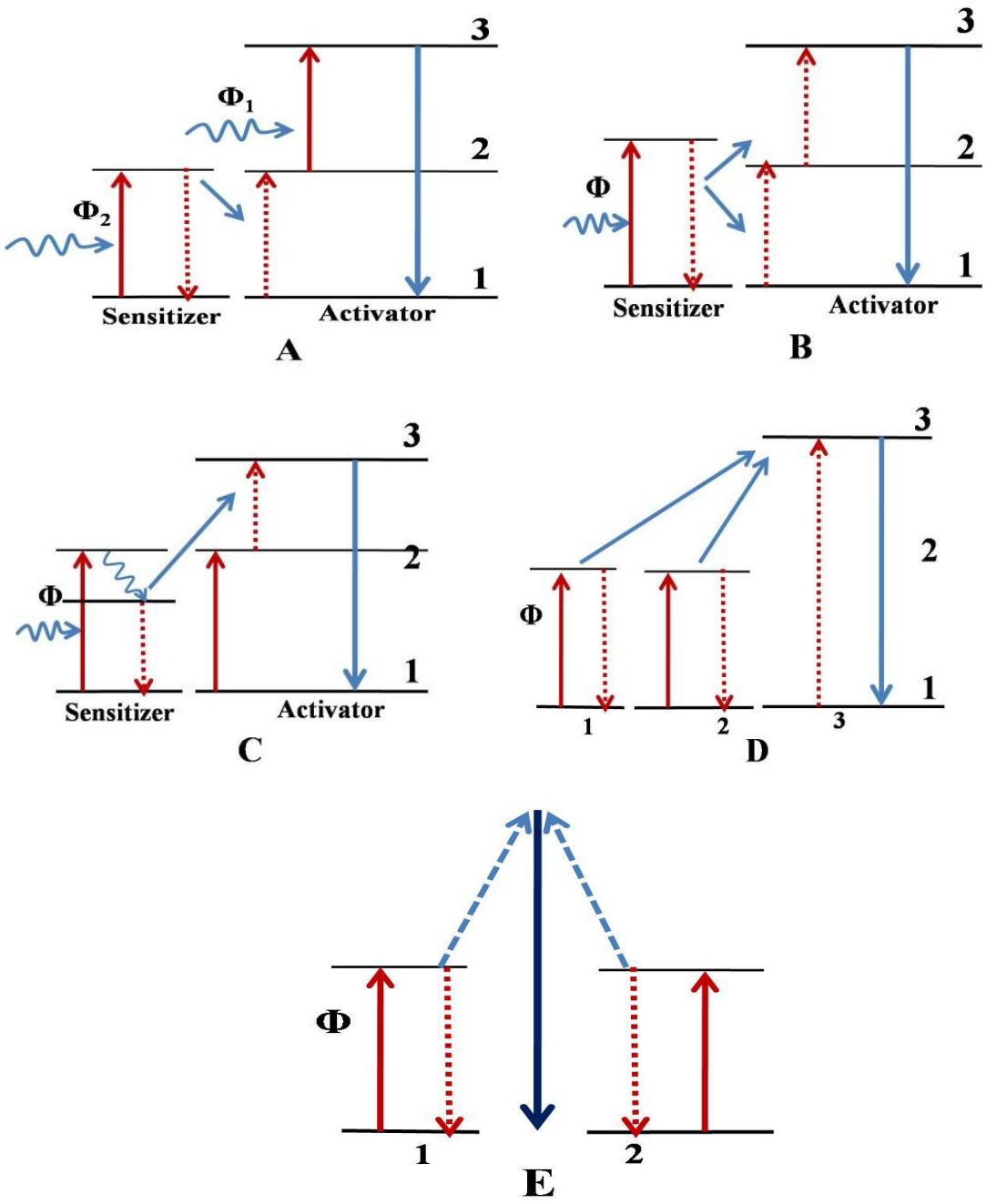

Figure 1.8: General energy schemes related to ETU processes: ET followed by ESA (A), successive energy transfer (B), cross-relaxation upconversion (C), cooperative sensitization (D), and cooperative phenomenon (E).

Except for case-A, the incident photons need to be resonant with only one transition; therefore, they may be provided by the same source. The anti-Stokes emission intensity (I) is thus proportional to Φ_2 and, more generally, it is proportional to the n^{th} power of Φ for an *n*-step process. The time dependence of the anti-Stokes fluorescence depends on the relaxation rates of the intermediate states and on the ET probability. As all these processes involve the interaction between two RE ions, they depend on the RE ion concentration in the host. Any mismatch between the energy levels of the sensitizer and

that of the activator can be counter balanced by phonons. In practice, energy difference considerations are used to identify the type of ETU. This may also allow a method to distinguish between ET and ESA.

ETU as an upconversion laser pumping process has advantage over ESA as only one pump beam is necessary, thus permitting a simpler pumping configuration. However, RE concentration in the host should be high enough so that ion–ion interactions can induce ET.

1.10.3 Photon avalanche (PA)

The PA phenomenon was first discovered by Chivian, et al. (1979) in Pr^{3+}: $LaCl_3$/$LaBr_3$ materials. Pr^{3+}-doped $LaCl_3$ or $LaBr_3$ crystal was pumped by the radiation from a continuous-wave (cw) dye laser at a frequency which matches the $^3P_1 \leftarrow {}^3H_5$ transition. If the incident intensity is slightly above a certain critical intensity, Pr^{3+} fluorescence originating from the $^3P_1$ or $^3P_0$ relaxation is enlarged by orders of magnitude, and correspondingly, a significant decrease in the pump intensity is observed. This phenomenon is an example of efficient cross-relaxation ET between the lowest IR levels of Pr^{3+}, which populates the $^3H_5$ state and thus makes the ESA process useful for quantum counter.

As PA excites ions to an excited state whose excitation energy exceeds that of the pump photon, clearly it may be used to obtain anti-Stokes emissions. Figure 1.9 shows a simple energy scheme for a PA process. This is an unconventional pumping mechanism because it may lead to strong upconverted emission from level 3 without any resonant ground-state absorption (GSA). The pump wavelength is resonant between a metastable state 2 and a higher energy level, and this is a characteristic of PA.

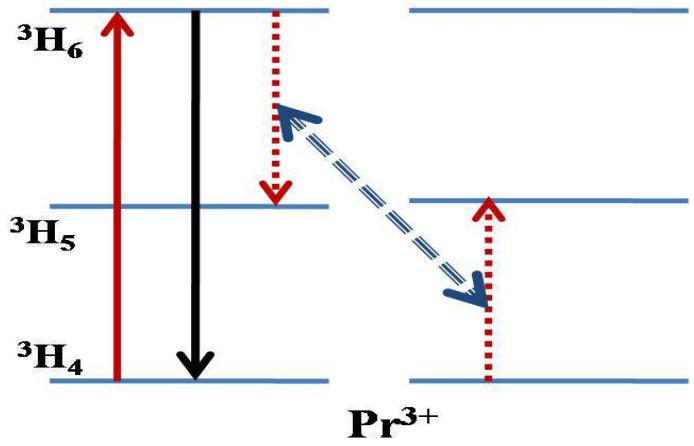

Figure 1.9: Energy scheme for the simplest photon avalanche process.

Another characteristic of PA is an excitation power threshold, which as was observed experimentally clearly separates two different regimes. Below the threshold, the upconverted fluorescence intensity is weak, and the crystal is transparent to the pump beam. Above the threshold, the fluorescence increases by orders of magnitude, and the pump light is strongly absorbed. There is also a change in the shape of the transient signal. The existence of such an excitation power threshold clearly identifies the PA different from ESA or ETU.

1.11 Energy Transfer between Rare-Earth Ions in Solids

ET is an important optical process that controls the luminescence of a material. When the concentration of active ions is increased in the solid, energy is transferred between the active ions due to the formation of ion pairs or any significant modifications in the radiative transition probabilities. Such an ET can take place by several ways as discussed below.

1.11.1 Resonant radiative energy transfer

An efficient ET process requires a significant spectral overlap between the emission of a donor and the absorption of an activator. If a radiative ET occurs predominantly, the decay time of the sensitized luminescence does not vary with the activator concentration. [Figure 1.10]

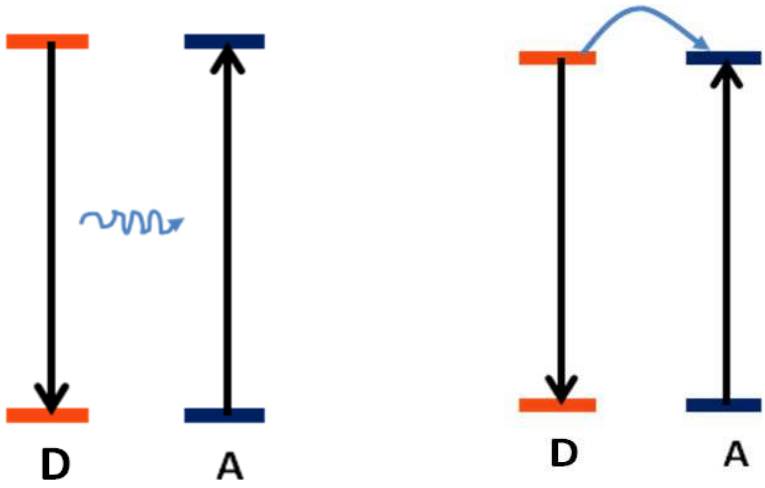

Figure 1.10: Resonant (a) radiative energy-transfer and (b) nonradiative energy transfer processess.

1.11.2 Resonant nonradiative energy transfer

The nonradiative ET is often accompanied by a significant decrease in the decay time of sensitized luminescence versus activator concentration. Two other lines of evidence for the occurrence of nonradiative ET are as follows: (i) the presence of an

excitation band of the sensitizer in the excitation spectrum of the activator and (ii) the presence of activator emission observed in the emission spectrum when the sensitizer is selectively excited (Figure 1.10 (b)).

1.11.3 Phonon-assisted energy transfer

In phonon-assisted ET, considerable mismatch may occur between the excitation energies of the acceptor and sensitizer. In this process, the energy released by the sensitizer is absorbed by the acceptor, which is excited to A^*, and simultaneously to conserve energy, a phonon of energy ħω is absorbed or emitted (Figure 1.11).

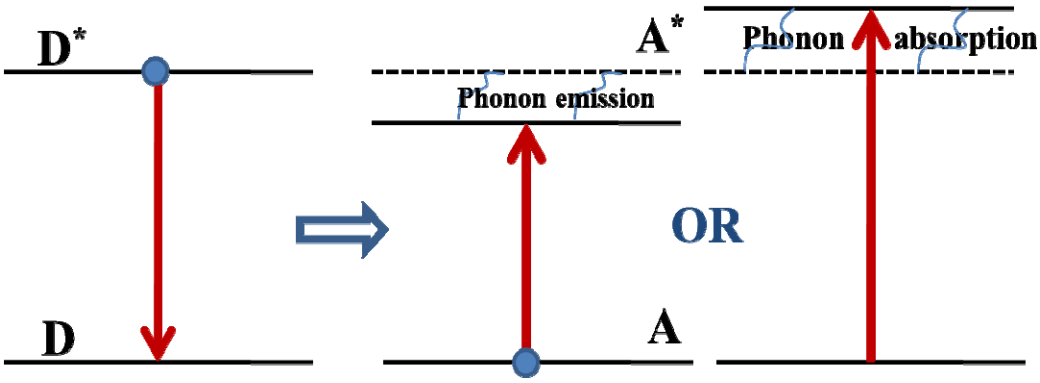

Figure 1.11: Nonresonant energy-transfer process.

1.11.4 Ion-pair emission and absorption

In the case of ion-pair emission, D decays from its excited state D^* to its ground state, and simultaneously ion A is excited from its ground state to its excited state A^*. Simultaneously, a photon of energy $D^* \rightarrow A^*$ is emitted. In the case of ion-pair absorption, the absorption occurs from excited state A^* to excited state D^*, transferring ion D from its ground state D to excited state $D^*$and ion A from its excited state A^* to the ground state. The mechanism is shown in Figure 1.12.

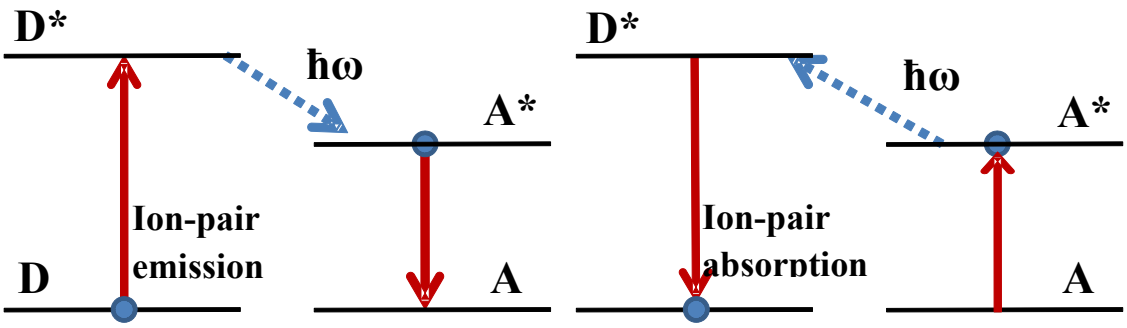

Figure 1.12: Ion-pair emission and absorption processes.

In radiative ET as shown in Figure 1.10(a), photons are emitted by the sensitizer ions (D) and are absorbed by the activator ions (A). The photons must be able to travel unhindered between the two ions; therefore, such a transfer depends on the relative distance and stereoscopic arrangement of the ions. Moreover, according to the degree of overlap between the emission spectrum of the donor (D) and the absorption spectrum of the activator (A), the emission spectrum of the donor will change with the change in activator concentration, but the donor lifetime would remain unchanged. These features provide the criteria for distinguishing between radiative and nonradiative resonant ETs. The probability for such a transfer between two ions at a sufficiently large distance R can be expressed as follows [Auzel (2004)]:

$$p_{DA}(R) = \frac{\sigma_A}{4\Pi R^2 \tau_D} \int g_{D(\upsilon)} g_{A(\upsilon)} d\upsilon \tag{1.20}$$

where τ_D is the donor lifetime, σ_A the integrated absorption cross-section of the acceptor, $g_D(\upsilon)$ is the lineshape function for donor emission, $g_D(\upsilon)$ is the line shape for acceptor emission, and the integral represents the spectral overlap between the absorption of A and emission of D. R is the distance between the two ions, and the distance dependence is R^{-2}. Such a resonant radiative ET may permit the long-range energy diffusion between identical ions and results in photon-trapping. These light-trapping effects increase the apparent experimental lifetime; the real lifetime can be obtained using thin and lightly doped samples.

To understand nonradiative ET (ET), let us consider the simple case of two ions, each with one excitable electronic state separated from the respective ground state by almost equal energy as shown in Figure 1.10. In the presence of a suitable interaction, the interactive energy may be transferred from S to A before S has the chance to emit a quantum of fluorescence. The possible mutual interaction of interest is the Coulomb interaction of the van-der Waals type. Forster (1948) considered a dipole–dipole interaction and assumed that the interaction is stronger if both the transitions are electric dipole-allowed transitions [Dexter (1953)]. The interaction energy is then directly proportional to the inverse of the third power of the distance between the ions, and the ET probability can be expressed as follows:

$$\mathrm{P_{SA}} = \frac{2\pi}{h} \left| \left\langle S^* A^0 \middle| H_{SA} \middle| S^0 A^* \right\rangle \right|^2 \rho_E \tag{1.21}$$

where H_{SA} is the electric dipole–dipole interaction Hamiltonian, directly proportional to the inverse of the third power of ion–ion separation, and ρ_E is the density of the vibrational states contributing to the line broadening of the transition. The ET probability, P_{SA}, is thus proportional to the inverse sixth power of the ion separation. The wavefunction used in evaluating the matrix element describe the initial state of the system in which the sensitizer is in its excited state while the activator is in its ground state, and the final state has the sensitizer in its ground state and the activator is in its excited state. The ET probability can be expressed as follows:

$$P_{SA} = \frac{1}{\tau_S}\left(\frac{R_0}{R}\right)^6 \tag{1.22}$$

where τ_s is the actual lifetime of the sensitizer excited state, including multiphonon radiative decay, and R_o is the critical transfer distance for which the excitation transfer and spontaneous deactivation of the sensitizer have equal probability.

The ET probability for (electric) multipolar interactions can be generally expressed as follows [Dexter (1953)]:

$$P_{SA} = \frac{(R_0/R)^S}{\tau_S} \tag{1.23}$$

where S is a positive integer with the following values:

S = 6 for dipole–dipole interaction

S = 8 for dipole–quadrupole interaction

S = 10 for quadrupole–quadrupole interaction

For small sensitizer concentrations, the time dependence of the donor fluorescence signal intensity is given, based on a model suggested by Inokuti and Hirayama [Inokuti *et al.* (1965)] as follows:

$$I(t) = I_0 \exp\left[-\frac{t}{\tau_0} - \Gamma\left(1-\frac{3}{S}\right)\frac{c}{c_0}\left(\frac{t}{\tau_0}\right)^{\frac{3}{S}}\right] \tag{1.24}$$

where S = 6, 8, and 10 for electric dipole–dipole, dipole–quadrupole, and quadrupole–quadrupole interactions. Γ is the gamma function. τ_0 is the lifetime of the donor in the absence of an acceptor. From the fit of this equation to the observed decay, in principle, the value of S and hence the nature of the interaction can be determined.

It has been observed that for relatively large donor concentrations, the resonant exchange of energy between donor ions themselves also becomes important. The decay curve of the donor fluorescence assuming dipole–dipole interaction [Yokota *et al.* (1967)] can be described as follows:

$$I(t) = I(s)\exp\left\{-\frac{t}{\tau_0} - \sqrt{\left(\frac{1}{2}\right)\left(\frac{c}{c_0}\right)\left(\frac{t}{\tau_0}\right)^{\frac{1}{2}}\left[\frac{1+10.87y+15.5y^2}{1+8.743y}\right]^{\frac{3}{4}}}\right\} \quad (1.25)$$

where $y = D_F, \tau_S, R_o^{-2}\left(\frac{t}{\tau_0}\right)^{\frac{2}{3}}$, D_F is the diffusion constant, and τ_0 is the intrinsic sensitizer (donor) lifetime. For small *t*, this formula yields nonexponential decay. For large *t*, the diffusion becomes important, and an exponential decay occurs. The decay constant can be expressed as follows:

$$\frac{1}{\tau} = \frac{1}{\tau_0} + 4\pi D_F C R_S \quad (1.26)$$

where $R_s = 0.68\ (a_6 / D_F)^{7/4}$, C is the acceptor concentration, and $a_6 = \frac{R_0^{\ 6}}{\tau_S}$. Three regions for the donor concentration C_D are considered. For small donor concentrations, the donor–donor interaction is small, and the time dependence of the donor decay can be described by Eq. (1.25). For moderate concentrations, the migration (diffusion) becomes significant, and for small *t*, the decay is nonexponential, while for large t, an exponential diffusion-limited decay occurs. For very large donor concentrations, almost every excited donor may be the nearest neighbor to an unexcited donor, and an exponential decay determined by the nearest neighbor donor–donor transfer rate occurs.

1.12 Concentration Quenching

A general theory of concentration quenching was proposed by Dexter et al. (1954). According to this theory, if the activator (acceptor) concentration increases above a critical concentration, the mutual distance between the activator ions becomes so small that an ET between these ions becomes possible, and the excitation energy can migrate through the lattice to different sites (killer sites) where this energy is lost nonradiatively. These killer sites may be impurities, defects, surface sites, etc. Therefore, the intensity of the fluorescence is significantly reduced. A concentration-dependent lifetime and fluorescence intensity measurements can indicate the presence

of concentration quenching and the operating ET mechanism. The fluorescence yield of RE ions increases with increasing dopant concentration up to a certain concentration, beyond which any increase in the concentration decreases the yield. The lifetime of the fluorescing state also shows a similar behavior.

1.13 Multiphonon De-excitation

A major channel for the nonradiative decay of excited ions is multiphonon de-excitation where the excited ion relaxes into the lower energy levels, releasing a part of its energy in terms of phonons. The rate of this process strongly depends on the electron–phonon coupling of the ion involved. The single-configurational coordinate model is used as a starting point for calculating the multiphonon decay rate [Yen, et al. (2006)]. The rate is a complex function of the number p of the phonons of energy ħω needed to bridge the energy gap ΔE (p = ΔE/ħω) and the Huang–Rhys parameter S. The multiphonon decay rate, if the energy gap (ΔE) is much larger than the phonon energy ħω), can be expressed as follows [Layne (1977)]:

$$W_{nr} = B(n(T) + 1)^{p} \exp(p \ln n) \qquad (1.27)$$

where B: material constant

n(T): phonon occupancy number, $n(T) = (\exp(\hbar\omega /kT) - 1)^{-1}$

n: electron–phonon coupling constant (n < 1)

Because of the exponential dependence on the number p (= ΔE/ ħω) of phonons, the decay rate across a given energy gap is determined mostly by the highest energy phonons that the host material supports. The highest phonon energy in common host materials is in the range of from ~300 cm^{-1} for some fluoride crystals to 1300 cm^{-1} for some silica-based glasses. The emission from an energy level will be strongly quenched if less than five phonons can span the energy gap to the next lower level. The transition is predominantly radiative if seven or more phonons are needed.

1.14 Current Research Trends on Up and downconversion Phosphors

Although RE upconversion phosphors have potential utility, the practical use of upconversion was primarily focused on bulk glasses or crystals for the past four decades. The low upconversion efficiency of the nanomaterials limits their pervading applications of the phosphors. The challenges are how to synthesize highly dispersible and uniform nanocrystals with strong upconversion emission in aqueous media.

Now-a-days, upconversion nanophosphors with good efficiency can be prepared routinely, and thus the study of upconversion processes has evolved into a highly interdisciplinary field covering photochemistry, biophysics, solid-state physics, and materials science. Furthermore, the phosphors can still be improved in terms of their stability against severe environment, chemicals, upconversion efficiency, color purity, etc.

Also current research is going on search of single phasic nanophosphor material which can be potentially applicable in WLEDs technology for lightening. RE ions are used as spectral converting materials in enhancing the efficiency of Si solar cell through downshifting, down and upconversion processes.

Low-phonon-frequency hosts are important to achieve high up and down conversion efficiency, and the studies in this direction are underway. From the most recent studies and their respective aims, some future trends and perspectives can be described to better understand some of the observed features. In the following section, they will be divided into three main expected directions:

- Upconversion-based lasers
- Downconversion-based materials for WLEDs
- Optical temperature sensors

Aim of the Thesis

The objective of this thesis is to identify novel titanate and molybdate-based low-phonon-frequency hosts as highly efficient up and downconversion phosphors and their applications. We have selected $Y_2Ti_2O_7$ and $CaMoO_4$ as the hosts for doping of RE ions into the host matrix.

Er^{3+}, Eu^{3+}, and Yb^{3+} ions were selected as the active centers. Er^{3+} gives intense emission in green and red regions. Yb^{3+} ion was used as the sensitizer for other ions by 976-nm diode laser pumping.

Eu^{3+} has generally been selected as the activator ion to investigate the luminescence properties of rare earth doped materials as it shows brilliant emission in the visible region. Since ground electronic state configuration of Eu^{3+}ion has $^7F_0$ non degenerate and having non-overlapping $^{2S+1}L_J$ multi-plets. Therefore Eu^{3+} ion can be used as a structural probe for investigating the local environment in a host matrix.

This scientific understanding will help the development of these materials for suitable optical applications.

★★★★★★